

**CONSTRUCTION OF AN OPTICAL CT SCANNER FOR
ACCESSIBILITY IN THE CLASSROOM**

An Undergraduate Research Scholars Thesis

by

MADISON WHITE

Submitted to the LAUNCH: Undergraduate Research office at
Texas A&M University
in partial fulfillment of requirements for the designation as an

UNDERGRADUATE RESEARCH SCHOLAR

Approved by
Faculty Research Advisor:

Mary P. McDougall, Ph.D.

May 2023

Major:

Biomedical Engineering

Copyright © 2023. Madison White.

RESEARCH COMPLIANCE CERTIFICATION

Research activities involving the use of human subjects, vertebrate animals, and/or biohazards must be reviewed and approved by the appropriate Texas A&M University regulatory research committee (i.e., IRB, IACUC, IBC) before the activity can commence. This requirement applies to activities conducted at Texas A&M and to activities conducted at non-Texas A&M facilities or institutions. In both cases, students are responsible for working with the relevant Texas A&M research compliance program to ensure and document that all Texas A&M compliance obligations are met before the study begins.

I, Madison White, certify that all research compliance requirements related to this Undergraduate Research Scholars thesis have been addressed with my Faculty Research Advisor prior to the collection of any data used in this final thesis submission.

This project did not require approval from the Texas A&M University Research Compliance & Biosafety office.

TABLE OF CONTENTS

	Page
ABSTRACT.....	1
ACKNOWLEDGEMENTS.....	2
1. INTRODUCTION	3
1.1 Background and Significance.....	3
1.2 Research Questions and Objectives.....	5
2. METHODS	7
2.1 Materials	7
2.2 Imaged Subjects.....	9
2.3 Code for Reconstruction.....	10
2.4 Comparison of Resolution Across Simplifications	15
3. RESULTS	19
3.1 Initial OCT simplification	19
3.2 Second OCT simplification	28
3.3 Third OCT simplification.....	32
3.4 Modification and its Effect on Resolution.....	36
3.5 Application in the Greater Scope of Medical Imaging.....	42
4. CONCLUSION.....	45
4.1 Ability of the System to be Modified for Accessibility.....	45
4.2 Effect of Simplification on Resolution.....	45
4.3 Proven Application in Education.....	46
4.4 Summary.....	46
REFERENCES	48

ABSTRACT

Construction of an Optical CT Scanner for Accessibility in the Classroom

Madison White
Department of Biomedical Engineering
Texas A&M University

Faculty Research Advisor: Dr. Mary P. McDougall
Department of Biomedical Engineering
Texas A&M University

Medical imaging technology and methods constitute an entire field of research, industry, and academia in biomedical engineering. The development of technology has awarded us the ability to see how the body works without invasive measures. Allowing for improved ease and succinct detection, medical imaging is imperative to the diagnosis and treatment of diseases within the body. Education on this topic holds equal importance and added difficulty in attempting to move from abstract to tangible learning. With the expense and wide inaccessibility associated with medical imaging machines, there is a further challenge in the ability to learn through an interactive experience. To combat this, the following work constitutes educational discovery within optical imaging and the limits of accessibility. An optical CT scanner can be constructed using attainable and accessible materials for less than \$100, with a smartphone used for image acquisition. The simplicity and accessibility of constructing an imaging device allow for tangible learning through assembly. As technology in engineering progresses, so does the inaccessibility to materials and education. As a result of this research, I hope to provide an interactive and compelling educational opportunity that is inexpensive and attainable.

ACKNOWLEDGEMENTS

Contributors

I would like to thank my faculty advisor, Dr. Mary P. McDougall, and the graduate students in the laboratory for their guidance and support throughout the course of this research.

Thanks also go to my friends and colleagues and the department faculty and staff for making my time at Texas A&M University a great experience.

The data analyzed for comparison in section 3.6, Application in the Greater Scope of Medical Imaging, was provided by graduate students in the Texas A&M NMR laboratory, Edith Valle and Jacob Degitz.

All other work conducted for the thesis was completed by the student independently.

Funding Sources

This project has received funding from the NMR RF Lab.

1. INTRODUCTION

1.1 Background and Significance

1.1.1 *Imaging Technology and Methods*

Imaging technology and methods refer to the development of various technologies that are used to measure, manipulate, and monitor biological and physiological parameters within living systems [1]. It is a critical field of research, industry, and academia in biomedical engineering, and it holds significant importance in healthcare. Imaging technological tools have been instrumental in the diagnosis and treatment of various medical conditions, and hold critical significance in research and development in the field of health care.

One of the primary advantages of imaging technology and methods is that they help healthcare professionals identify abnormalities and ensure more accurate diagnoses. For example, instruments such as electrocardiograms and blood glucose monitors are commonly used to monitor heart activity and blood sugar levels, respectively, which allows doctors to detect any abnormalities and provide timely intervention. With advancements in technology, monitoring tools have become more sophisticated, allowing healthcare providers to detect even the slightest physiologic changes that may require medical attention.

Medical imaging and the development of technology and methods has awarded the ability to see how the body works without invasive discovery. Allowing for improved ease and succinct detection, innovation in imaging technology and methods has allowed for the optimization of modern treatment.

1.1.2 Optical Imaging

Optical imaging is a non-ionizing and non-invasive technology that uses light as the basis of its functionality, allowing for a high spatial resolution to provide quantitative information [2]. It is a vital area of research within imaging technology, as the contrast of optical imaging affords information about the structure, function, and degree of transparency of single-celled tissues to the entirety of an organism [3].

The ability to study the function of living organisms in optical imaging provides contrasting information when compared to other imaging modalities, allowing for real-time and quantitative monitoring [2]. Additionally, due to its lack of ionizing radiation, non-invasive nature, and high-resolution images, optical imaging allows for a unique opportunity for educational study.

1.1.3 Computed Tomography

A computed tomography (CT) scan offers tomographic images with detailed information of a specific area in a cross-section of the imaged subject [6]. Unlike traditional X-rays, CT imaging can visualize imaged subjects in three dimensions rather than two following post-processing image acquisition.

Tomography, the method by which CT images are produced, requires reconstruction due to the nature of image acquisition occurring in multiple angles and planes. The nature of tomography allows for high-resolution images that provide information about the location and function of structures within the body.

Imaging modalities such as single-photon emission computerized tomography (SPECT), positron emission tomography (PET), CT, and magnetic resonance imaging (MRI) utilize tomographic techniques for image acquisition and processing [7]. The implementation of

tomographic experimentation through this project is therefore a useful tool for gaining an introductory understanding of the underlying concepts that form the foundation of many imaging technologies. It provides an opportunity to explore the principles of tomography and the ways in which they can be applied to various imaging modalities.

1.1.4 Inaccessibility

Education on medical imaging and imaging technology and methods hold equal importance and added difficulty in an attempt to move from abstract to tangible learning. With the expense and wide inaccessibility associated with medical imaging machines, there is a further challenge in the ability to learn through an interactive experience.

As a result of this research, I hope to provide an interactive and compelling educational opportunity that is inexpensive and attainable. In the educational field of medical imaging, it is difficult to move from abstract to reality. With the expense and wide inaccessibility associated with medical imaging machines, there is a further challenge in the ability to learn through an interactive experience. As the technology in engineering progresses, so does the inaccessibility to materials and education. In the making of an optical CT scanner using attainable materials, students gain the opportunity to learn through construction. With adjustments to previous research, education in optical imaging is adjusted to be accessible and tangible to students.

1.2 Research Questions and Objectives

The simplicity and accessibility of the construction of an imaging device allow for tangible learning through assembly. This project aimed to build upon the previous work of [4], which describes the construction of an optical CT scanner. An optical CT scanner can be constructed using attainable and accessible materials, allowing this work to be further simplified with only a few necessary components. In [4], materials call for a USB camera, a LED lamp light

source, and a computer that can read images as the subject rotates. Initially, this work was adjusted to allow for a smartphone with video capability to be the image capture device. Along with this, a single kit was purchased to provide rotation of the subject and act as the light source. However, still requiring purchases and technology with software capability, the following questions were posed:

1. Can the scanner be simplified to allow for the construction to consist of nearly fully found materials?
2. Does the improvement of accessibility reduce the degree of resolution provided by the scanner?
3. What educational topics can be addressed by the construction of a simplified OCT system?

By discovering the limits of simplification in the name of accessibility, the quality of results will be assessed and compared. With the focus on the act of constructing the machine and carrying out the imaging of subjects, open-source code will be provided for the 3D reconstruction. Through the establishment of limitations, the scope that the project is extended under will allow for great education freedom and adaptability.

2. METHODS

2.1 Materials

2.1.1 *First Simplification*

To begin the process of simplifying previous research, a tomographic imaging system based on visible light was constructed using a range of components, including an ELEGOO UNO R3 Microcontroller Board (EL-CB-001) for communication with the Arduino Editor program. Additional components included an MB102 Breadboard Power Supply Module, an LED light source, and an ELEGOO ULN2003 Stepper Motor Driver Board (EL-SM-003), all of which were connected to the ELEGOO Solderless Breadboard (EL-CP-003). The ELEGOO Stepper Motor (EL-SM-003) was wired directly to the driver board.

The microcontroller board used in the circuitry works to dictate a specific function in a device by interpreting the data it receives using its central processor. The temporary information is stored in its memory, where the processor accesses and applies the received data. The board's I/O peripherals then communicate and enact the needed action [8]. The breadboard power supply module converts the computer-supplied power to 5 or 3.3 volts depending on need. The stepper motor, a DC motor that moves in discrete steps, has multiple coils that are organized in groups called "phases". Each phase is energized in sequence, allowing the motor to rotate one step at a time [9]. The driver board applies voltage to each of the coils in a specific sequence and allowed the connection between the motor and the computer interface [9].

To create the scanner casing, ¼" white acrylic cuttings were utilized, with the inside painted black to isolate the system from external light. Additionally, two camera linear polarizers were cut from the Linear Polarization A4 Sheet Polarizer (ki399) and placed just before and after

the imaged object. To ensure a more homogeneous light beam, a semitransparent film was placed directly in front of the light source to act as a diffuser.

To capture the images, a smartphone time-lapse video was implemented, with the imaged subject rotating by 2 degrees per second. After the subject was imaged, it was removed from the system and a background image was taken to allow for subtraction from the rest of the images. This method provided a means of image capture that was both effective and efficient.

2.1.2 Second OCT simplification

With the knowledge that any box that isolates outside light can be used, components can be purchased separately or as a kit, a smartphone can be used, and any object with transparency can be imaged, the initial optical tomographic imaging system was further simplified. Using pieces of found cardboard, the outside casing was constructed into a box for use as the scanner. The inside was painted black to allow for isolation from external light and reflection, and two camera linear polarizers were cut again from the Linear Polarization A4 Sheet Polarizer and placed just before and after where the object would be imaged. A piece of parchment paper was cut and stretched to be used in place of the semi-transparent film. An ELEGOO UNO R3 Controller Board was used again for communication with the Arduino Editor program, along with a MB102 Breadboard Power Supply Module, an LED light source and an ELEGOO ULN2003 Stepper Motor Driver Board circuited to the ELEGOO Solderless Breadboard. Using the ELEGOO Stepper Motor wired to the driver board, a smartphone video was the means of image capture and the imaged subject was rotated by 2 degrees per second. After the subject was imaged, it was removed from the system and a background image was taken to allow for subtraction from the rest of the images.

2.1.3 Third OCT simplification

To address the issue of the unavailability of a purchased stepper motor kit, further simplifications were made to the construction of the visible light-based tomographic imaging system. Using the previously constructed box, cardboard pieces were used again to construct the outside scanner casing, which was painted black to ensure isolation from external light and reflection. Camera linear polarizers were again cut from the Linear Polarization A4 Sheet Polarizer and placed just before and after where the object was to be imaged. A piece of parchment was used once more to replace the semi-transparent film. It was realized that the code could extract each video frame, making the 2 degrees per second rotation rate unnecessary, which allowed the object to be manually rotated by hand. After the subject had been imaged, it was removed from the system and a background image was taken to allow for subtraction from the rest of the images: a necessary step. For the light source, a LED lamp found in the laboratory was utilized, but any other available light source, such as a second flashlight-capable smartphone, could be used as well. Overall, these simplifications and adaptations highlight the versatility and flexibility of the visible light-based tomographic imaging system, making it accessible and affordable for a wide range of users and applications.

2.2 Imaged Subjects

With less consideration taken of medical application, a focus was put instead on the capability of the constructed machines. Three subjects were chosen to be imaged: a red gummy bear, a section of a cotton ball, and a vial of gelatin with air bubbles added before solidification. While not holding medical applications, the imaging of the red gummy bear and the vial of gelatin fit the criteria of semi-transparency, while having high-detail topographic and internal aspects. The section taken from the cotton ball allowed for semi-transparency with a non-light

diffusing feature, allowing for exploration of how the presence of the dense sections of cotton and other non-light diffusing objects would affect the information we could receive from the subject.

2.3 Code for Reconstruction

As the method of image capture was a taken video and not a captured image at each degree of rotation, each frame of the captured video needed to be isolated. The following MATLAB code provided a method to extract each frame of the video taken of the subject. As shown below in algorithm 1, the code reads in the video, extracts each frame, and saves it to a folder that the user names. In this case, the tomographic “slice” was the two-dimensional image at its specific angle in time. Rather than having an image captured at every two degrees of rotation, extracting an image from a video allowed for full rotation of the subject, with additional splices for increased resolution.

Algorithm 1: Extract each frame from taken video

```
1  % Reads the video and assigns it to a variable
2  v = VideoReader('chosen_video.mp4'); %Where “chosen_video” is located, user will input path to
3  % video on desktop
4
5  % Determines the number of frames in the video
6  numFrames = v.NumberOfFrames;
7
8  % Prompts the user to input the name the folder which will store the extracted images on the desktop
9  folderName = input('Enter the name of the folder where the extracted images will be saved: ', 's');
10 folder = fullfile(getenv('USERPROFILE'), 'Desktop', folderName);
11 if ~exist(folder, 'dir') % Saves images to existing folder if already in files
12     mkdir(folder);
13 end
14
15 % Extracts each frame and save it as a jpg file in the new folder
16 for i = 1:numberFrames
17     frame = read(v,i);
18     filename = fullfile(folder, sprintf('frame%d.jpg', i));
19     imwrite(frame, filename);
20 end
```

Following a successful extraction of each image from the video, the background image taken at the end of imaging needed to be removed from each slice. This allowed for images that solely constituted the imaged subject, and set up the process needed for successful 3D reconstruction.

Algorithm 2: Remove the background image from each slice

```

1  % Specify the desktop directory path so that background images will be saved to the desktop
2  desktop_dir = fullfile(pwd, 'Desktop');
3
4  % Prompts the user to select the background image file by navigating them to their files
5  [bg_file, bg_path] = uigetfile(fullfile(desktop_dir, '*.*'), 'Select the background image file');
6  background_image = imread(fullfile(bg_path, bg_file)); % Assigns a variable to background image
7
8  % Prompts the user to select the directory containing the images to process
9  img_path = uigetdir(desktop_dir, 'Select the directory containing the images to process');
10 image_files = dir(fullfile(img_path, '*.jpg')); % Can change if images are different than jpg
11
12 % Creates a new file on the desktop to save the processed images
13 output_dir = fullfile(desktop_dir, 'processed_images');
14 if ~exist(output_dir, 'dir') % Saves images to existing folder if already in files
15     mkdir(output_dir);
16 end
17
18 % Reads through each image file in the chosen folder
19 for i = 1:numel(image_files)
20     % Reads in the image
21     image_filename = fullfile(img_path, image_files(i).name);
22     image = imread(image_filename);
23
24     % Removes the background from the image using the imsubtract function
25     foreground = imsubtract(image, background_image);
26
27     % Save the foreground image in the output folder with a new _foreground added to file name
28     [~, image_name, image_ext] = fileparts(image_filename);
29     foreground_filename = fullfile(output_dir, [image_name, '_foreground', image_ext]);
30     imwrite(foreground, foreground_filename);
31 end

```

As each still image extracted from the video needed to have the same axis of rotation and be centered on that axis to allow for successful three-dimensional reconstruction, the following code provided needed corrections.

Algorithm 3: Correct the axis of rotation and centers the image

```

1  % Sets the input and output folder paths

```

```

2  input_folder_path = 'C:\Users\user\foreground images'; % Images obtained from algorithm 2
3  output_folder_path = 'C:\Users\user\corrected images'; % Where the corrected images will go
4
5  % Creates the output folder if it does not exist
6  if ~exist(output_folder_path, 'dir')
7      mkdir(output_folder_path);
8  end
9
10 % Creates a list of all the image files in the input folder
11 image_files = dir(fullfile(input_folder_path, '*.jpg'));
12
13 % Reads through each image and corrects its orientation and position
14 for i = 1:length(image_files)
15     % Read the image
16     image_path = fullfile(input_folder_path, image_files(i).name);
17     image = imread(image_path);
18
19     % Convert the image to grayscale
20     gray_image = rgb2gray(image);
21
22     % Binarize the image
23     binary_image = imbinarize(gray_image);
24
25     % Find the properties of the objects in the image
26     stats = regionprops(binary_image, 'MajorAxisLength', 'Orientation', 'Centroid');
27
28     % Get the major axis length and orientation of the largest object
29     [~, max_idx] = max([stats.MajorAxisLength]);
30     major_axis_length = stats(max_idx).MajorAxisLength;
31     orientation = stats(max_idx).Orientation;
32     centroid = stats(max_idx).Centroid;
33
34     % Correct the orientation of the major axis to be 90 degrees
35     angle_diff = 90 - orientation;
36     rotated_image = imrotate(image, angle_diff, 'crop');
37
38     % Calculate the new position of the major axis
39     [rows, cols, ~] = size(rotated_image);
40     new_center = [cols/2, rows/2];
41     old_center = centroid;
42     dist = norm(new_center - old_center);
43     translation = new_center - old_center;
44
45     % Translate the image to center the major axis
46     translated_image = imtranslate(rotated_image, translation, 'OutputView', 'full');
47
48     % Crop the image to remove any black borders
49     cropped_image = imcrop(translated_image, [0, 0, cols-1, rows-1]);
50
51     % Save the corrected image to the output folder
52     [~, filename, ext] = fileparts(image_files(i).name);

```

```

53 output_filename = sprintf('%s_corrected%s', filename, ext);
54 output_path = fullfile(output_folder_path, output_filename);
56 imwrite(cropped_image, output_path);
57
58 end

```

After ensuring that the obtained corrected splices of the imaged subject were centered and corrected on the axis of rotation, results were run through the following MATLAB code which reads in the corrected jpg images, stores them in a structured array, and creates individual sinograms for each image by converting the image to grayscale and using the built-in ‘radon’ function. A reconstruction array is then used to reconstruct a 3D volume from the sinograms, which is stored in the user’s computer.

Algorithm 4: 3D Reconstruction

```

1 % Reads path to desired images
2 input_folder_path = 'C:\Users\user\corrected images'; % Images obtained from algorithm 3
3 output_file = 'C:\Users\user\output\file.mat'; % Folder to save reconstruction
4
5 % Reads in the JPG images from the input folder
6 image_files = dir(fullfile(input_folder_path, '*.jpg'));
7 num_images = length(image_files);
8
9 % Creates a cell array to store the sinograms
10 sinograms = cell(num_images, 1);
11
12 % Gets the desired sinogram size based on the overall sinogram
13 theta = linspace(0, 180, 30600);
14 num_angles = length(theta);
15 num_detectors = size(radon(rgb2gray(imread(fullfile(input_folder_path, image_files(1).name))),
16 theta), 1);
17
18 % Loops through each image to create a sinogram
19 for i = 1:num_images
20 image_path = fullfile(input_folder_path, image_files(i).name);
21 image_data = rgb2gray(imread(image_path));
22 sinogramm = radon(image_data,theta);
23 % Resize sinogram to match theta size
24 sinograms{i} = imresize(sinogramm, [num_detectors, num_angles]);
25 end
26
27 % Concatenates the sinograms into an overall sinogram
28 overall_sinogram = cat(2, sinograms{:});
29
30 % Reconstructs the 3D image from the overall sinogram

```



```

31 reconstruction = zeros(floor(num_detectors/2), floor(num_detectors/2), floor(num_detectors/2));
32 for slice_idx = 1:num_detectors/2
33     slice = iradon(overall_sinogram(:, :, slice_idx), theta, 'linear', 'Ram-Lak', 1, num_detectors);
34     reconstruction(:, :, slice_idx) = slice(1:2:end, 1:2:end);
35 end
36
37 % Saves reconstruction
38 save(output_file, 'reconstruction');

```

Finally, algorithm 5 describes the MATLAB code needed to generate an overall sinogram image. This algorithm was extracted from the overall 3D reconstruction MATLAB code, as the computing time was high. Isolating this section of the code allowed for sinogram exploration without the needed computing time for algorithm 4.

Algorithm 5: Overall sinogram for extracted images.

```

1 % Set the path to the folder which holds the images obtained from algorithm 3
2 corrected_image_path = 'C:\Users\user\corrected_images'
3
4 % Reads in each image from the chosen folder
5 image_files = dir(fullfile(corrected_image_path, '*.jpg')
6 num_images = length(image_files);
7
8 % Creates a cell array to store the sinograms to be created
9 sinograms = cell(num_images, 1);
10
11 % Reads through each image and create an individual sinogram for each
12 theta = 0:179;
13 for i = 1:num_images
14     image_path = fullfile(corrected_image_path, image_files(i).name);
15     image_data = rgb2gray(imread(image_path));
16     sinograms{i} = radon(image_data, theta);
17 end
18
19 % Concatenates the sinograms into an overall sinogram by horizontally stacking
20 overall_sinogram = cat(2, sinograms{:});
21
22 % Displays the overall sinogram in grayscale
23 figure;
24 imagesc(overall_sinogram);
25 colormap(gray);
26 colorbar;

```

2.4 Comparison of Resolution Across Simplifications

The red gummy bear was chosen as the subject for resolution comparison due to the high tomographic details present. The gummy bear was imaged in the same controllable conditions for each optical CT scanner simplification. The same phone took a time-lapse video with 1080-pixel resolution at 30 frames per second. Images were extracted using the same code, and run through the same reconstruction program shown by algorithm 3.

The rate of rotation varied for each of the subjects. For the first and second OCT simplification, the imaged subject was rotated at 2 degrees per second with the help of the implemented stepper motor. However, the third OCT simplification called for manual rotation. Although control was attempted, the rotation throughout the third OCT simplification was inconsistent and more difficult to be calculated and marked. Along with this, it was more difficult to maintain the subject's location in space within the casing.

To answer question 2 in the proposed research questions and objectives: "Does the improvement of accessibility reduce the degree of resolution provided by the scanner?", MATLAB code was produced to allow for comparison. The chosen subject to compare the resolution and functionality of the machine was the gummy bear due to the high amount of tomographic offered.

Initially, the dimensions were taken from each image derived from algorithm 1, which extracted each of the still image's frames for the "slice" as a means of image acquisition, across each imaged subject and each system simplification. This is shown below in algorithm 6.

Algorithm 6: Determination of dimensions and pixels

```
1  Allows the user to select an image file
2  [file, path] = uigetfile('*.jpg', 'Select an image file');
3
4  % Reads the image file into a matrix
5  image_data = imread(fullfile(path, file));
6
```

```
7 % Determines the pixel size of the image
8 [height, width, num_channels] = size(image_data);
9
10 % Determines pixel per inch resolution
11 info = imfinfo(fullfile(path, file));
12 ppi = info.XResolution;
13
14 % Displays results
15 fprintf('Image dimensions: %d x %d x %d\n', height, width, num_channels);
16 fprintf('Image resolution: %d ppi\n', ppi);
```

After ensuring that image dimensions were consistent across the three imaged subjects, pixels per inch of each of the images were determined. If dimensions were found inconsistent, images were resized to be uniform across the three simplifications. The determination of resolution by pixels per inch was incorporated into the algorithm shown above. As the method of image acquisition stayed consistent across the three OCT machines, it was assumed that this would be unchanged across simplifications. However, it was a necessary aspect to be checked and the first quantifier on if accessibility affected the degree of resolution of the imaged subject.

Secondly, qualitative information was taken from each imaged subject. Markers were chosen to determine if information across simplifications was translated with increased accessibility. The gummy bear presented with four distinct protrusions or its “limbs”. This was chosen as the first marker. Along with this, the ability to distinguish the gummy bear’s facial features was chosen as a separate marker. The last chosen marker was the air bubbles the gummy bear contained, created during its gelatinizing process. The ability to discern the presence of these air bubbles gave us information on the resolution across simplifications.

Lastly, three images were chosen across the machine simplifications in which the gummy bear contained approximately the same orientation. Algorithm 6 was implemented to ensure that each of the images contained the same initial dimensions. Next, MATLAB code was created to

determine the size of the object within the frame. This accounted for the distance of the subject from the camera across imaging and is shown by algorithm 7 written below.

Algorithm 7: Determination of the size of the image within the frame

```
1 % Reads the image
2 img = imread("C:\Users\ image.jpg"); % Change the path to required image
3
4 % Converts image to grayscale and binarizes
5 bw_img = imbinarize(rgb2gray(img), 'adaptive', 'ForegroundPolarity', 'dark', 'Sensitivity', 0.5);
6
7 % Removes small objects and fill holes
8 bw_img = bwareaopen(bw_img, 100);
9 bw_img = imfill(bw_img, 'holes');
10
11 % Finds the largest connected object within the image (gummy bear)
12 largest_cc = bwpropfilt(bw_img, 'Area', 1, 'largest');
13
14 % Calculates the size of the largest connected object in pixels
15 size_in_pixels = sum(largest_cc(:));
16
17 disp(['Size in pixels: ' num2str(size_in_pixels)]); % Displays pixel count
```

To determine if there was a difference in object resolution and without solely attributing variances to distance from the camera, the isolated resolution of the object within the image was calculated across the OCT simplifications. This process was added to algorithm 7 shown above and created the final code shown below by algorithm 8. This was the final determination for comparison of resolution.

Algorithm 8: Determination of PPI resolution of the individual object in image

```
1 % Reads the image
2 img = imread("C:\Users\ image.jpg"); % Change the path to required image
3
4 % Converts image to grayscale and binarizes
5 bw_img = imbinarize(rgb2gray(img), 'adaptive', 'ForegroundPolarity', 'dark', 'Sensitivity', 0.5);
6
7 % Removes small objects and fill holes
8 bw_img = bwareaopen(bw_img, 100);
9 bw_img = imfill(bw_img, 'holes');
10
11 % Finds the largest connected object within the image (gummy bear)
12 largest_cc = bwpropfilt(bw_img, 'Area', 1, 'largest');
13
14 % Calculate the size of the largest connected object in pixels
15 size_in_pixels = sum(largest_cc(:));
```

```
16
17 % Calculates the size of the largest connected object in inches
18 resolution = 96; % Change for resolution found by algorithm 6
19 width_inches = size_in_pixels / resolution;
20 height_inches = size_in_pixels / resolution;
21
22 % Calculates the PPI resolution of the largest connected object
23 width_pixels = size(largest_cc, 2);
24 height_pixels = size(largest_cc, 1);
25 ppi_width = width_pixels / width_inches;
26 ppi_height = height_pixels / height_inches;
27 mean_ppi = (ppi_width + ppi_height) / 2;
28
29 % Displays the results
30 disp(['Size in pixels: ' num2str(size_in_pixels)]);
31 disp(['PPI resolution (width): ' num2str(ppi_width)]);
32 disp(['PPI resolution (height): ' num2str(ppi_height)]);
33 disp(['Mean PPI resolution: ' num2str(mean_ppi)]);
```

3. RESULTS

3.1 Initial OCT simplification

The initially constructed optical CT scanner and system returned a total cost of \$95.24 with a construction time of approximately 12 hours and an imaging time per subject of approximately 5 minutes. This initial system can be seen below in Figure 1.

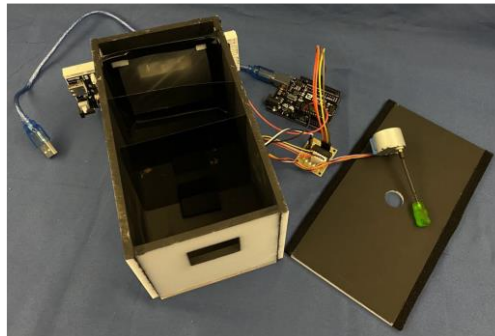


Figure 1: First constructed OCT system.

With initial imaging methods, 3 subjects were imaged: a red gummy bear, a section of cotton ball, and a vial of gelatin containing air bubbles added before solidification. While not holding medical applications, the imaging of these subjects fit the criteria of semi-transparency and touched upon various aspects of non-transparency, high tomographic detail, and high internal detail. Additionally, choosing consistency across the selection of imaged subjects allowed for later comparison of resolution.

Still images extracted from the first system and using algorithm 1 can be seen below in figures 2, 3, and 4.



Figure 2: Still of the red gummy bear from the initial OCT simplification



Figure 3: Still of the section of cotton ball from the initial OCT simplification



Figure 4: Still of the vial of gelatin with air bubbles added before solidification from the initial OCT simplification

After each of the stills had been extracted from the acquired video, algorithm 2 worked to remove the background information from each of the frames, leaving just the foreground. The resulting foreground images can be seen below in figures 5, 6, and 7.



Figure 5: Foreground image of the red gummy bear from the initial OCT simplification



Figure 6: Foreground image of the section of cotton ball from the initial OCT simplification



Figure 7: Foreground image of the vial of gelatin from the initial OCT simplification

Next, algorithm 3 worked to correct the axis of rotation of the image and center it in the frame. The results of this algorithm for the three image subjects for the initial OCT simplification can be seen below in figures 8 and 9 which show a specific frame from the extracted vial image before correction and after being put through the algorithm.



Figure 8: Still of the vial foreground before correction



Figure 9: Still of the vial foreground after correcting the axis of rotation and centering

Following the needed corrections achieved by algorithm 3, algorithm 5 was conducted on the corrected images to achieve a collective sinogram. Sinograms contain all of the necessary information needed for 3D reconstruction, and are a useful educational tool in the greater scope of tomographic imaging. Shown in figures 10, 11, 12, and 13 are the collective sinograms of the red gummy bear, the section of cotton ball, and the vial of gelatin achieved from the initial OCT simplifications.

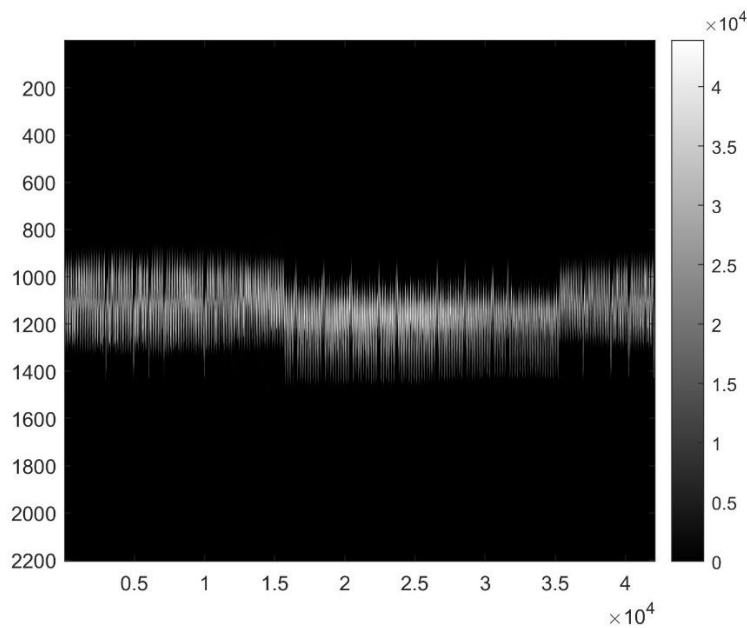


Figure 10: Sinogram of the red gummy bear (Initial OCT simplification)

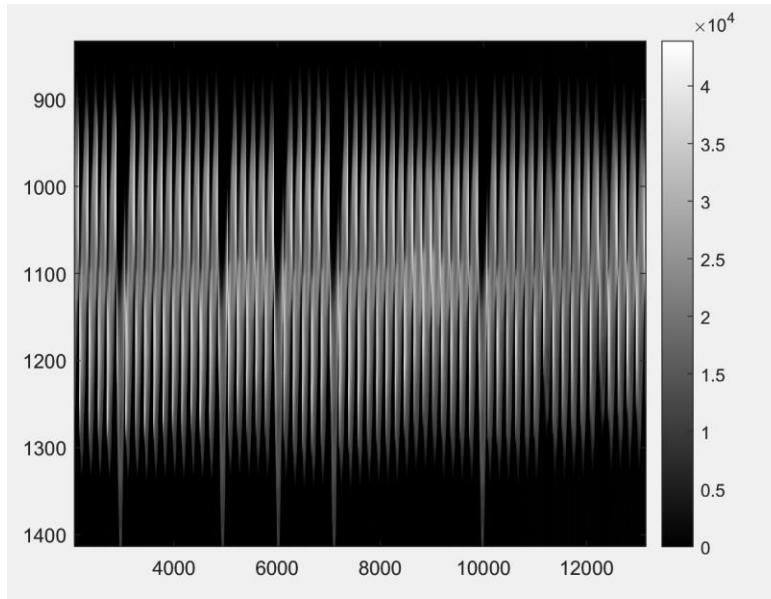


Figure 11: Separate view of the sinogram of the red gummy bear (Initial OCT simplification)

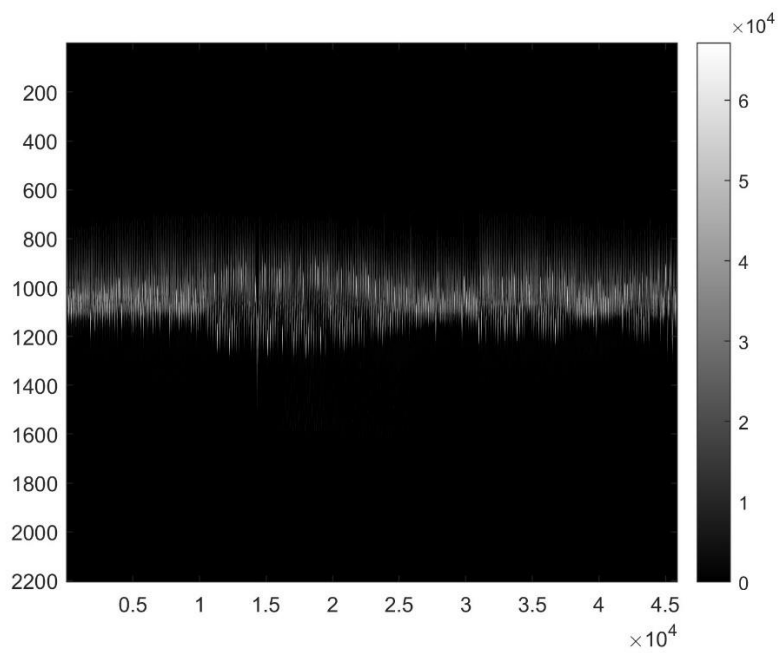


Figure 12: Sinogram of the vial of gelatin (Initial OCT simplification)

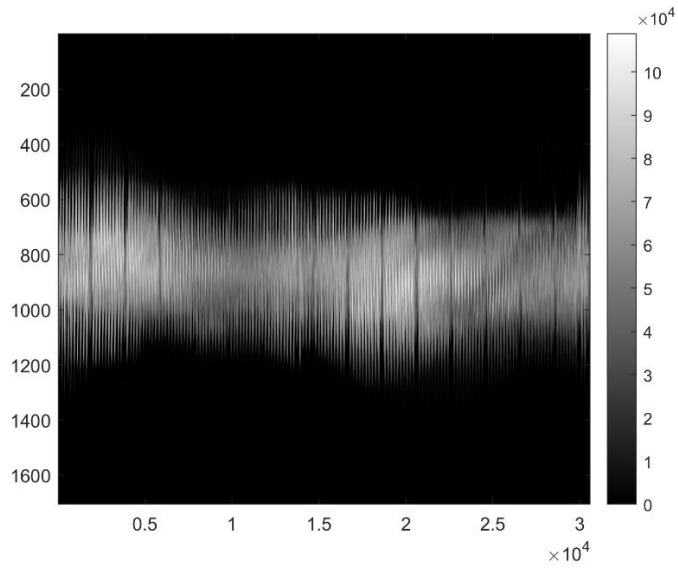


Figure 13: Sinogram of the cotton ball (Initial OCT simplification)

Lastly, the images obtained from algorithm 3 were processed using algorithm 4, which offered us the needed 3D reconstruction. Shown below in figures 14, 15, and 16 are the reconstruction images developed of the imaged gummy bear.

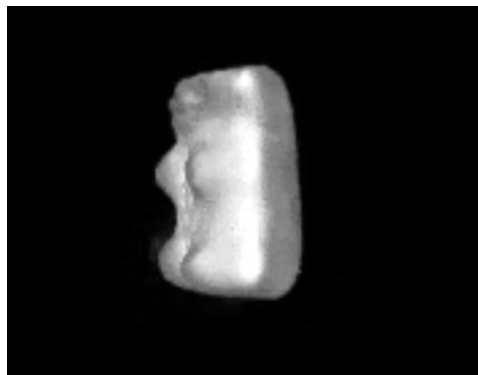


Figure 14 3D Reconstruction of the red gummy bear from the first OCT simplification



Figure 15: 3D Reconstruction of the red gummy bear from the first OCT simplification

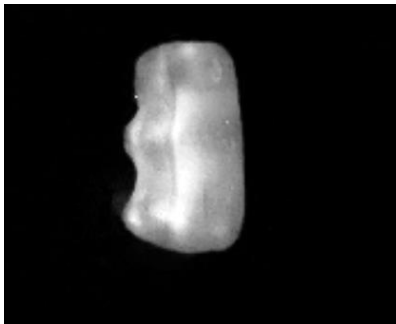


Figure 16 3D Reconstruction of the red gummy bear from the first OCT simplification

Shown below in figures 16 and 17 are the reconstruction images developed of the imaged vial of gelatin. The air bubbles present within the vial offered interesting internal information about the imaged subject. Problems with masking can be seen in figure 16, which shows a section of the object missing after being incorrectly removed by algorithm 2.

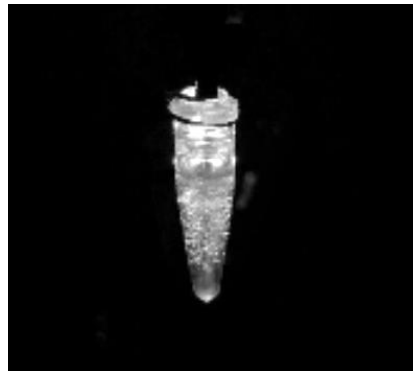


Figure 17: 3D Reconstruction of the vial of gelatin from the first OCT simplification



Figure 18: 3D Reconstruction of the vial of gelatin from the first OCT simplification

Shown below in figures 18 and 19 are the reconstruction images developed of the imaged section of the cotton ball. As can be seen, the axis of rotation was inconsistent across extracted frames, likely due to the indefinite and loosely defined shape of the object. This led to a reconstruction that did not result in a consistent circular view. Additionally, non-light diffusing aspects were inconsistent across perspectives. While this did not constitute a successful reconstruction, it gave valuable information on the limitations of the OCT machines.



Figure 19: 3D Reconstruction of the section of cotton ball from the first OCT simplification

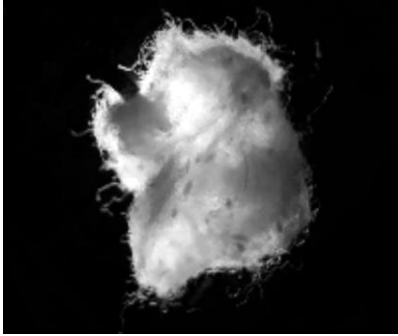


Figure 20: 3D Reconstruction of the section of cotton ball from the first OCT simplification

3.2 Second OCT simplification

Following modifications added in section 2.1.2, the second constructed optical CT system returned a total cost of \$34.87. The total construction time was approximately 2 hours, with an imaging time of approximately 5 minutes per subject. This simplified system can be seen below in figures 21 and 22.

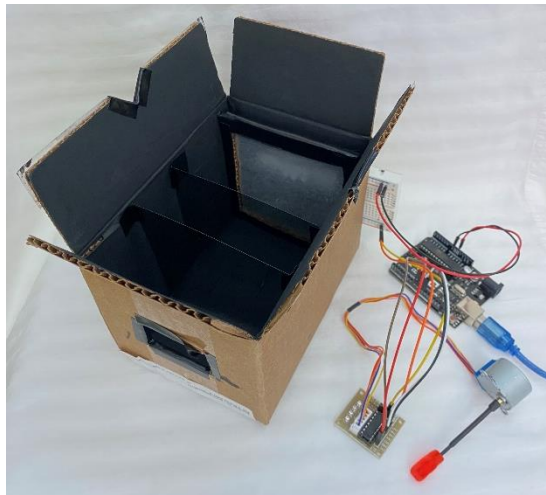


Figure 21: Second OCT simplification: Internal view

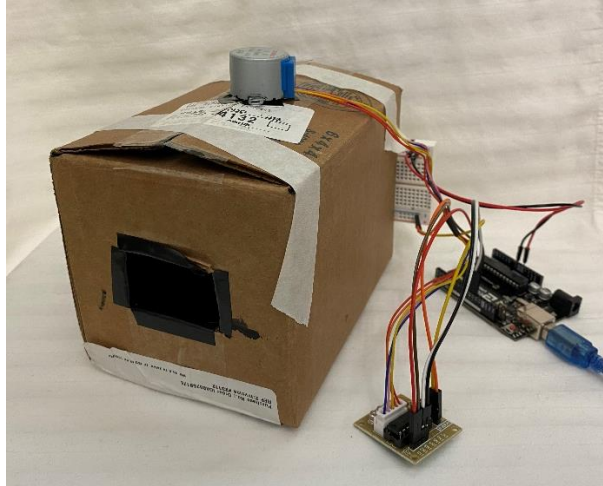


Figure 22: Second OCT simplification: View during imaging

As the question of interest pertained to resolution, the chosen subject of interest for imaging was the same red gummy bear imaged in the initial OCT simplification. A still image extracted from the second system before manipulation is shown below in figure 23.



Figure 23: Still of the red gummy bear from the second OCT simplification

After each of the stills had been extracted from the acquired video, algorithm 2 worked to remove the background information from each of the frames, leaving just the foreground. As can be seen, in figure 24, a greater number of artifacts existed within the image, making the

foreground calculation more challenging. As such, the initial masking of the background image did not result in a fully isolated foreground.

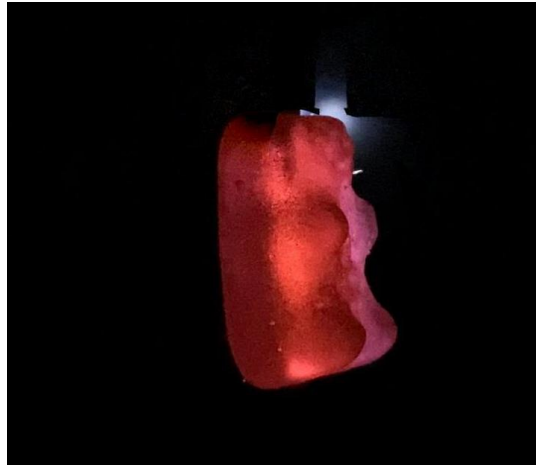


Figure 24: First attempt at background subtraction of the red gummy bear from the second OCT simplification

To correct this, a manual mask was created which highlighted the remaining artifacts for an improved foreground image. An example of the resulting image can be seen below in figure 25, with an example shown in figure 26 of the same frame after being processed by algorithm 3 to correct the axis of rotation and center it in the frame.



Figure 25: Final foreground image of the red gummy bear from the second OCT simplification

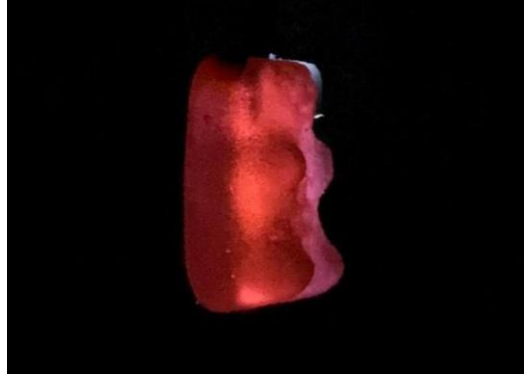


Figure 26: Corrected foreground image of the red gummy bear from the second OCT simplification

Following the needed corrections achieved by algorithm 3, algorithm 5 was conducted on the corrected images to achieve a collective sinogram. Shown in figure 27 is the collective sinogram of the red gummy bear.

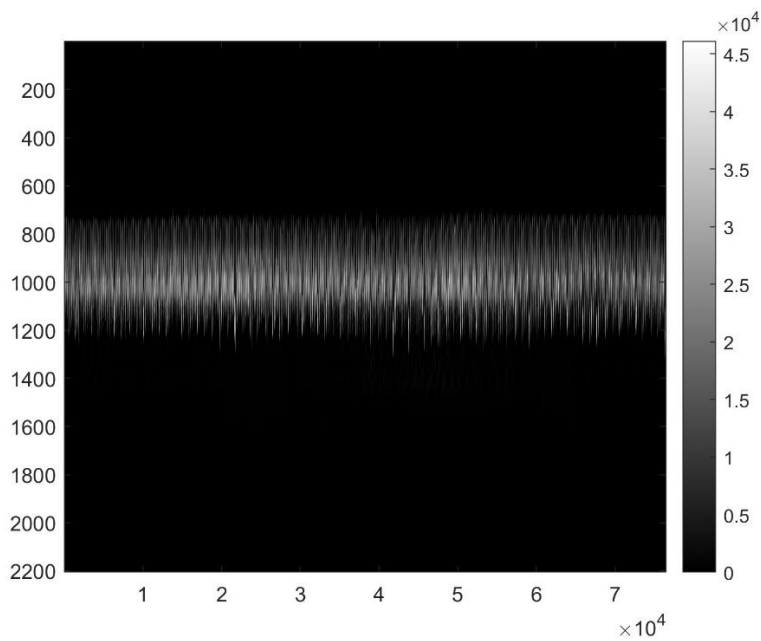


Figure 27: Sinogram of the red gummy bear (Second OCT simplification)

Lastly, the images obtained from algorithm 3 were processed using algorithm 4, which offered us the needed 3D reconstruction. Shown below in figures 28 and 29 are the 3D reconstruction images developed of the imaged gummy bear.

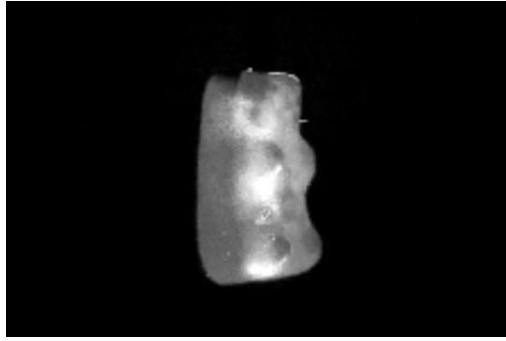


Figure 28: 3D Reconstruction of the red gummy bear from the second OCT simplification

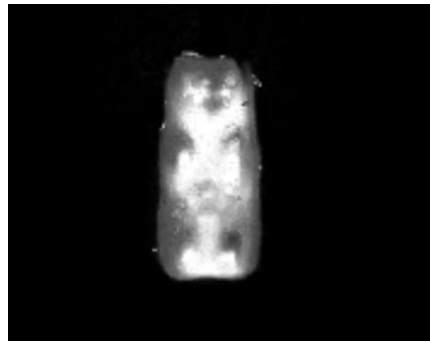


Figure 29: 3D Reconstruction of the red gummy bear from the second OCT simplification

3.3 Third OCT simplification

Following modifications added in section 2.1.3, the third constructed optical CT system returned a total cost of \$21.70. The total construction time was approximately 2 hours, with an imaging time of approximately 5 minutes per subject. The final modified system can be seen below in figures 30 and 31.



Figure 30: Third OCT simplification: View during imaging

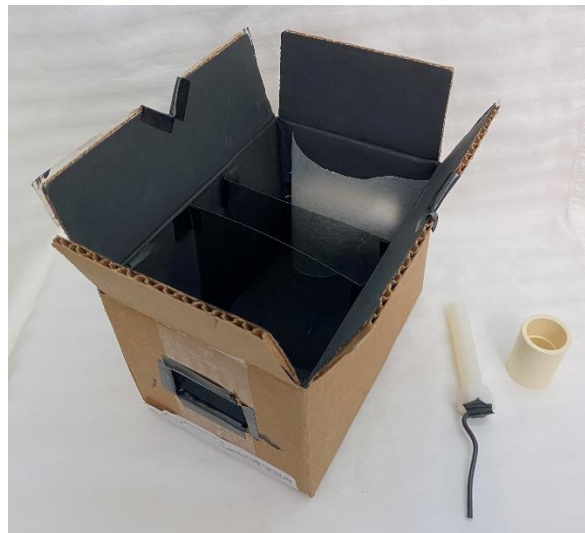


Figure 31: Third OCT simplification: Internal view

As the question of interest was resolution, the chosen subject of interest for imaging was the same red gummy bear imaged in the initial and second OCT simplification. A still image extracted from the third system before manipulation is shown below in figure 32.



Figure 32: Still of the red gummy bear from the third OCT simplification

After each of the stills had been extracted from the acquired video, algorithm 2 worked to remove the background information from each of the frames, leaving just the foreground. As can be seen above, the difference in lighting source created a more challenging foreground production. The greater intensity of light highlighted the accessible boxes' lessened ability to isolate light. As a result, a greater number of artifacts existed within the image with the first foreground removal, ensuing manual background removal being a necessity across the directory of images. The resulting image, along with the correction of the axis of rotation and centering, can be seen below in figure 33.

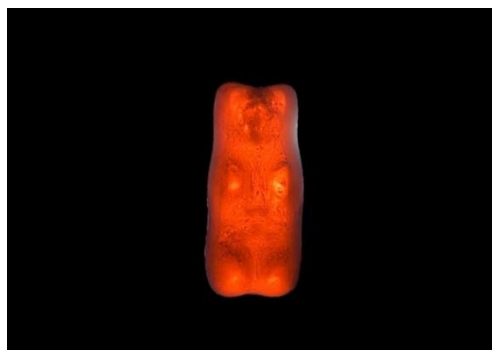


Figure 33: Corrected foreground image of the red gummy bear from the third OCT simplification

Following the needed corrections achieved by algorithm 3, algorithm 5 was conducted on the corrected images to achieve a collective sinogram. Shown in figure 34 is the collective sinogram of the red gummy bear.

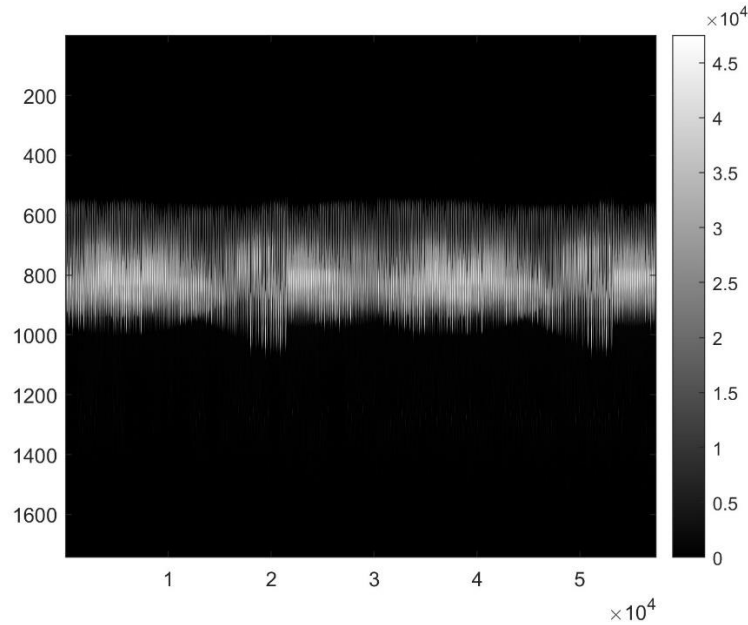


Figure 34: Sinogram of the red gummy bear (Third OCT simplification)

Lastly, the images obtained from algorithm 3 were processed using algorithm 4, which offered us the needed 3D reconstruction. Shown below in figures 35 and 36 are the 3D reconstruction images developed of the imaged gummy bear. As can be seen, while the higher light intensity allowed for a better result in the image extracts, it resulted in a lower resolution for the 3D reconstruction.



Figure 35: 3D Reconstruction of the red gummy bear from the third OCT simplification

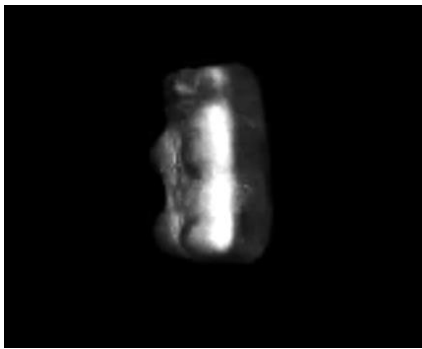


Figure 36: 3D Reconstruction of the red gummy bear from the third OCT simplification

3.4 Modification and its Effect on Resolution

3.4.1 Resolution of Initial OCT simplification

The dimensions of the stills extracted for the red gummy bear from the first simplification were determined to be 1920 pixels by 1080 pixels. The resolution, determined by pixels per inch, was determined to be 96.

To determine qualitative information taken from each imaged subject, four orientations of the red gummy bear were chosen for comparison. Taken from the images obtained by algorithm 3, these stills can be seen below in figure 37.

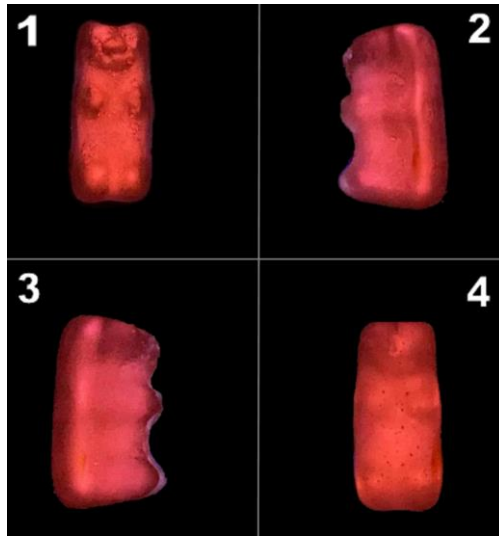


Figure 37: Four orientations chosen for comparison (initial OCT simplification)

Markers were chosen to determine if qualitative information across simplifications was translated with increased accessibility. The first marker, the gummy bear's limbs, was considered in the figures above. As shown by orientations 1, 2, and 3, the four limbs are clearly and easily distinguishable. The second marker, the gummy bear's facial features, was the second consideration. As shown by orientation 1, facial features are able to be discerned from the rest of the gummy bear. However, little information is given in orientations 2 and 3. The last chosen marker, the air bubbles the gummy bear contained created during its gelatinizing process, appear as texture across the four orientations. Shown in orientation 4, the air bubbles are discernable as black dots throughout the body of the gummy bear.

For the final determination of resolution for the initial OCT simplification, algorithms 7 and 8 were implemented to determine the size of the gummy bear in pixels as well as the resolution in terms of pixels per inch (PPI) of the object within the image. The same orientation of the forward-facing gummy bear was chosen across simplifications for uniformity. For the initial OCT simplification, the gummy bear returned a size of 45299 pixels after processing by

algorithm 7. Following processing by algorithm 8, the gummy bear returned a mean resolution of 3.1768 PPI after averaging the resolution of the height and width of the object.

3.4.2 Resolution of Second OCT simplification

The dimensions of the stills extracted for the red gummy bear from the second OCT simplification were determined to be 1920 pixels by 1080 pixels. The resolution, determined by pixels per inch, was determined to be 96. This was consistent with the initial OCT simplification and expected, as the method of imaging, the smartphone time-lapse video, was kept consistent across the three OCT simplifications.

For qualitative information across simplifications, markers were considered again. Taken from the images obtained by algorithm 3, four orientations of the red gummy bear from the second OCT simplification can be seen below in figure 38.

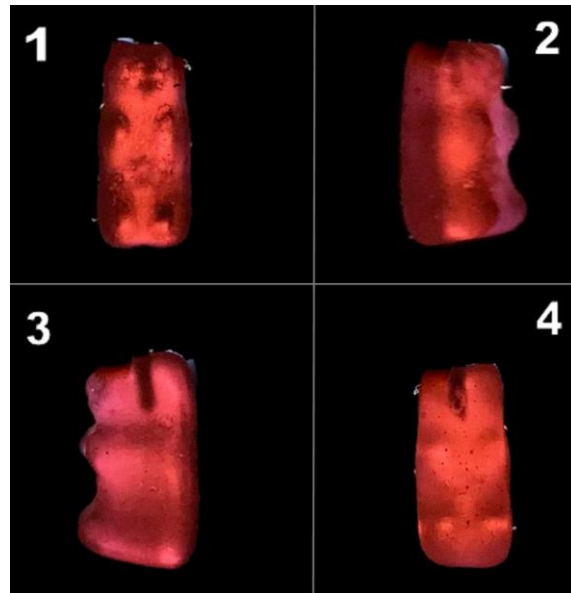


Figure 38: Four orientations chosen for comparison (second OCT simplification)

The first marker, the gummy bear's limbs, was considered in the figures above. As shown by orientations 1, 2, and 3, the four limbs were found easily distinguishable but were less sharply marked when compared to the initial OCT simplification. The second marker, the gummy bear's

facial features, was the second consideration. Orientations 1, 2, and 3 offer us little information on discernable facial features. Slight features can be distinguished in orientation 3, but are not clearly shown. Differences in surface tomography are recognized, but the nose and head separation from the remainder of the body is inadequate when compared to orientation 1 in figure 37. This visual comparison can be seen below in figure 39.



Figure 39: Differences in discernable facial features across the initial OCT simplification (left) and the second OCT simplification (right)

The last chosen marker, the air bubbles the gummy bear contained created during its gelatinizing process were less clear across the four orientations when considering the qualifier as a textured appearance. However, as shown in orientation 4, the air bubbles are more discernable as black dots throughout the body of the gummy bear than shown in orientation 4 in figure 37.

For the final determination of resolution for the second OCT simplification, algorithms 7 and 8 were implemented to determine the size of the gummy bear in pixels as well as the resolution in terms of pixels per inch (PPI) of the object within the image. The same orientation of the forward-facing gummy bear was chosen across simplifications for uniformity. For the second OCT simplification, the gummy bear returned a size of 47565 pixels after processing by algorithm 7. Following processing by algorithm 8, the gummy bear returned a mean resolution of 3.0254 PPI after averaging the resolution of the height and width of the object.

3.4.3 Resolution of Third OCT simplification

The dimensions of the stills extracted for the red gummy bear from the third OCT simplification stayed consistent with the first and second and were determined to be 1920 pixels by 1080 pixels. The resolution, determined by pixels per inch, was determined to be 96.

For qualitative information across simplifications, markers were considered for the final simplification. Taken from the images obtained by algorithm 3, four orientations of the red gummy bear from the third OCT simplification can be seen below in figure 40.

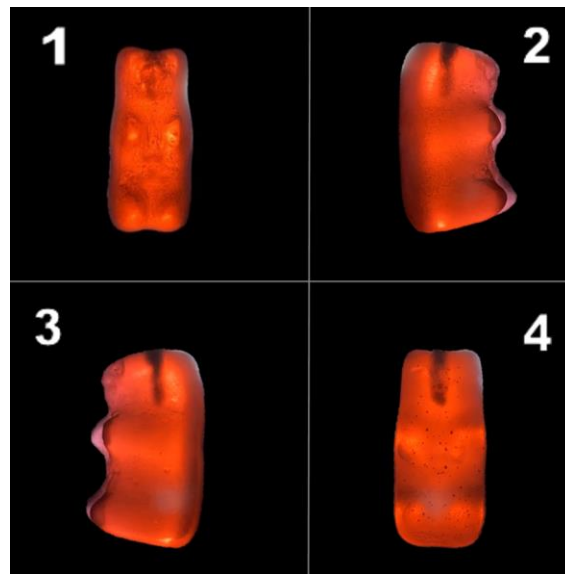


Figure 40: Four orientations chosen for comparison (third OCT simplification)

The first marker, the gummy bear's limbs, was considered in the figures above. Likely due to the higher intensity light source, the gummy bear's limbs were the most clearly shown in the third simplifications extracted images. As shown by orientations 1, 2, and 3, the four limbs are clearly and easily distinguishable. The second marker, the gummy bear's facial features, was the second consideration. As shown by orientation 3 in figure 40, this simplification offered us the best OCT image for facial distinction from the side orientations. However, as shown by orientation 1, the third simplification gave us the least amount of information about the facial

features present, appearing without texture. This comparison across the OCT simplifications can be seen below in figure 41.

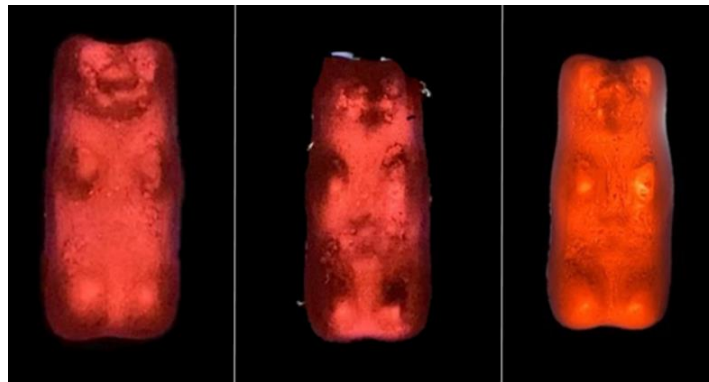


Figure 41: Differences in discernable facial features across the initial OCT simplification (left), the second OCT simplification (middle), and the third OCT simplification (right)

The last chosen marker, the air bubbles the gummy bear contained created during its gelatinizing process, were the most clearly distinguished in the third simplification. While not appearing as strongly as texture, individual air bubbles can be distinguished throughout the orientations. Shown in orientation 4, the air bubbles offer the greatest distinction as black dots throughout the body of the gummy bear than shown in the first and second OCT simplifications.

For the final determination of resolution for the third OCT simplification, algorithms 7 and 8 were implemented to determine the size of the gummy bear in pixels as well as the resolution in terms of pixels per inch (PPI) of the object within the image. The same orientation of the forward-facing gummy bear was chosen across simplifications for uniformity. For the third OCT simplification, the gummy bear returned a size of 98068 pixels after processing by algorithm 7. Following processing by algorithm 8, the gummy bear returned a mean resolution of 1.4723 PPI after averaging the resolution of the height and width of the object.

3.4.4 Overall Resolution Comparison Results

The initial comparison of dimensions and overall image resolution produced consistent results across simplifications. This was expected as the method of imaging, a smartphone time-lapse video, was consistent across the machines with the same smartphone.

Comparison of the visual aspects of the OCT machines proved to have advantages and disadvantages across machines. Some of the internal and tomographic aspects of the gummy bear were improved with the third simplification, which could be attributed to the light source with greater intensity and the subject being closer in proximity to the camera. However, it held disadvantages in the ability to discern facial features in the forward-facing orientation. The second simplification had the worst visual resolution results when compared to the initial and third OCT simplifications, demonstrating that greater modifications were necessary when establishing increased simplifications otherwise.

The individual calculation of resolution across the gummy bear subject when chosen from the same orientation had diminishing results across simplifications. This comparison can be seen below in table 1.

Table 1: Object resolution (PPI) across OCT simplifications

	Initial Simplification	Second Simplification	Third Simplification
Object Resolution	3.1768 PPI	3.0254 PPI	1.4723 PPI

3.5 Application in the Greater Scope of Medical Imaging

As a continuation of the project and as a proven application within the field of medical imaging research and the medical field, a phantom designed for use in MRI was comparatively

imaged against acquired optical CT images in an effort to discern the sources of the varying susceptibility effects. The phantom of interest was an agar phantom composed of 1.5% agarose, 3% NaCl, and undissolved CaCO₃ particles synthesized by graduate students in the lab. The purpose of the phantom was to mimic calcifications in ex vivo muscle tissue for an assessment of calcium as an early biomarker of disease progression in Duchenne Muscular Dystrophy (DMD).

MR images were obtained with a Varian Inova 4.7T research scanner, a spin echo pulse sequence, and a gradient echo sequence. The OCT images provided a reference for previously acquired MRI scans and allowed a comparison of visible susceptibility artifacts they could not discern as air bubbles or calcium deposits. The resulting assessment allowed improved determination of calcifications in the ex vivo muscle tissue and allowed the graduate students to discern the composition of specific inhomogeneities.

Figure 42 shows the images acquired with the MRI system, as well as the images acquired with the OCT system. The section labeled “A” in the figure shows the MR scan acquired with a gradient echo sequence which shows inhomogeneities by the boundaries between the phantom and air. The section labeled “B” in the figure shows an MR scan acquired with a spin echo sequence which corrects mentioned inhomogeneities. The section labeled “C” in the figure offers a comparison from the optical CT process.

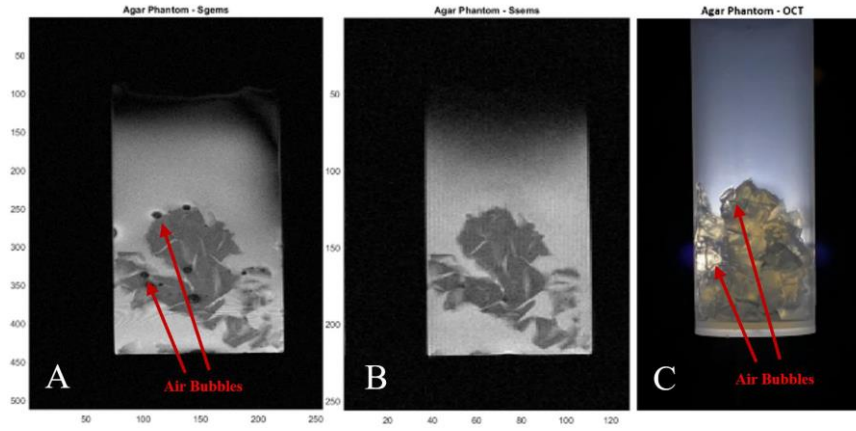


Figure 42: MR acquired scans as compared to optical CT acquired scans.

4. CONCLUSION

4.1 Ability of the System to be Modified for Accessibility

The initial cost of the first constructed optical CT system was \$95.24 and was able to be reduced to a total cost of \$21.70. The use of cardboard for the casing in the second and third OCT simplification gave flexibility in material choice and accounted for a student's inability to access more sophisticated resources. While the use of more accessible material for the casing resulted in a lessened ability to isolate external light, it did not reduce the functionality of the machine and led to greater tomographic exploration in the creation of manual masking. The use of parchment paper in the second and third OCT simplifications additionally incorporated the use of found materials and proved to be effective as the light-diffusing component. The nature of the post-processing in-house MATLAB code for reconstruction reduced the need for a purchased kit and electric rotation and accounted for a student's lack of financial capability or access to purchased components.

4.2 Effect of Simplification on Resolution

After completing the necessary manipulation techniques, the images were successfully compared against each other. While individual object resolution decreased across OCT simplifications, advantages existed in visual qualifiers across machines. Overall image resolution was consistent across the OCT modifications, and the variation between scanners allowed for the discovery of future improvements. For example, a light source with greater intensity allowed for increased topographical distinction as compared to the LED-circuited breadboard. The acrylic casings used in the initial simplification isolated external light more proficiently than the cardboard casing, and using the motor as the method of rotation allowed for more consistent

positioning of the subject. However, where these aspects were disadvantaged in the acquisition of images, the work to correct them allowed for compelling education exploration and learning. Overall, the improvement of accessibility reduced the individual degree of resolution provided by the scanner in the individual objects but offered advantages in visual qualifiers in resolution.

4.3 Proven Application in Education

This project was outlined and executed for use in my faculty advisor's medical imaging course. A rubric was constructed which allowed for freedom of material choice, kit purchase, and image acquisition. With the created open access code, there existed the potential for independent discovery and execution of post-processing image manipulation. Students not only gain valuable education on the manipulation of optical properties but can apply learned concepts on the principles of tomography and the ways in which they can be applied to various imaging modalities. Along with this, education on the topic of optical computed tomography can be applied to other imaging modalities, as shown in section 3.5. By gaining introductory knowledge through the construction of an OCT machine and image processing techniques, students gain a valuable baseline for entrance to the greater scope of medical imaging.

4.4 Summary

The development of a low-cost optical computed tomography (OCT) system with simplified materials and software has proven to be effective in improving accessibility and reducing the inaccessibility associated with hands-on imaging technology education. The application of this project in education provides students with valuable experience in the manipulation of optical properties and the principles of tomography, which can be applied to various imaging modalities such as magnetic resonance imaging, positron emission tomography, and optical coherence tomography. Overall, the project has demonstrated that the use of

accessible materials and open-source software can facilitate the construction of low-cost medical imaging systems, making education and research in this field more accessible and inclusive.

REFERENCES

- [1] “About,” UC Berkeley Department of Bioengineering. [Online]. Available: <https://bioeng.berkeley.edu/research/bioinstrumentation>.
- [2] E. M. Serrao, A. S. Thakor, V. Goh, and F. A. Gallagher, “Optical Imaging,” *Optical Imaging - an overview | ScienceDirect Topics*. [Online]. Available: <https://www.sciencedirect.com/topics/neuroscience/optical-imaging>.
- [3] E. M. C. Hillman, C. B. Amoozegar, T. Wang, A. F. H. McCaslin, M. B. Bouchard, J. Mansfield, and R. M. Levenson, “In vivo optical imaging and dynamic contrast methods for biomedical research,” *Philosophical transactions. Series A, Mathematical, physical, and engineering sciences*, 28-Nov-2011. [Online]. Available: <https://www.ncbi.nlm.nih.gov/pmc/articles/PMC3263788/>.
- [4] M. Orfanakis, “Tomography in school - Optical CT Scanner with Lego or Arduino,” *Science on Stage*, 2017. [Online]. Available: <http://www.science-on-stage.eu/material/tomography-school-optical-ct-scanner-lego-and-arduino>.
- [4] J. SL; “Optical properties of biological tissues: A Review,” *Physics in medicine and biology*. [Online]. Available: <https://pubmed.ncbi.nlm.nih.gov/23666068/>.
- [5] J. Battista, R. Taylor, K. Jordan, J. Miller, and I. MacDonald, “A portable optical CT scanner for interactive teaching of Medical Imaging principles,” *Scholarship@Western*. [Online]. Available: https://ir.lib.uwo.ca/wcse/WCSEEleven/Wed_July_6/20/.
- [6] P. R. Patel and O. De Jesus, “CT Scan,” *PubMed*, 2021. [Online]. Available: <https://www.ncbi.nlm.nih.gov/books/NBK567796/>
- [7] S. Hussain et al., “Modern Diagnostic Imaging Technique Applications and Risk Factors in the Medical Field: A Review,” *BioMed Research International*, vol. 2022, pp. 1–19, Jun. 2022, doi: <https://doi.org/10.1155/2022/5164970>.
- [8] B. Lutkevich, “What is a microcontroller and how does it work?,” *IoT Agenda*, 07-Nov-2019. [Online]. Available: <https://www.techtarget.com/iotagenda/definition/microcontroller>.

- [9] “Everything you need to know about Stepper Motors,” RS. [Online]. Available: <https://uk.rs-online.com/web/content/discovery/ideas-and-advice/stepper-motors-guide>.